JOURNAL OF MATERIALS SCIENCE 30 (1995) 5652–5656

Creep and densification during anisotropic sintering of glass powders

A. R. BOCCACCINI*‡, D. M. R. TAPLIN*‡, P. A. TRUSTY§, C. B. PONTON*§
School of Metallurgy and Materials, and § IRC in Materials for High Performance Applications, University of Birmingham, Birmingham B15 2TT, UK

The isothermal sintering behaviour of a barium magnesium aluminosilicate glass powder at 930 °C was investigated using a heating microscope. The cylindrical samples exhibited a variable shrinkage anisotropy during sintering. The shrinkage anisotropy ratio, defined as the ratio of the relative change of height and diameter, varied linearly between ~0.3 and ~0.98 with the relative volume shrinkage during densification. Shrinkage anisotropy caused creep deformation of the samples. The creep rate varied exponentially with the densification rate and the ratio of creep to densification rates, $\dot{\varepsilon}_c/\dot{\varepsilon}_\rho$, decreased as densification proceeded. This is in disagreement with most previous studies, which show a constant value of $\dot{\varepsilon}_c/\dot{\varepsilon}_\rho$ during the densification. Overall, the study points out the relevance of variable shrinkage anisotropy and how it affects the densification behaviour of glass powders.

1. Introduction

Densification prior to crystallization, i.e. a glass-ceramic route, is expected to be particularly important for forming high-density composites by pressureless sintering. At an equivalent inclusion content, glass matrices have been shown to exhibit a much higher sinterability compared to crystalline matrices [1, 2] and therefore the beneficial sintering characteristics of glass can be conveniently exploited. This fact has renewed interest in understanding the sintering of glasses under different conditions.

The simultaneous creep and densification of glass powder compacts has been studied in the past and a fundamental understanding of the evolution of both mechanisms (i.e. creep and densification) under different experimental conditions has been gained [3–6]. Most studies have been conducted using loading dilatometric measurements, i.e. applying controlled low uniaxial loads to the sintering compact. One of the important results of this work is that the creep rate can be expressed as the sum of the contribution from the applied stress which varies linearly with the stress and a contribution due to anisotropic densification. It was shown that the latter varied linearly with the densification rate for compacts which shrank more in the axial than in the radial direction [3]. Another interesting result is that the ratio of the densification to the creep rate is almost independent of both temperature and density for a given applied stress [3, 4]. This result was later confirmed for pressureless sintered samples, i.e. samples densified under no applied stress [6, 7]. All the experimental studies on creep/densification of glass powder compacts carried out so far have dealt with samples which showed constant shrinkage anisotropy during densification. It has been shown in the literature, however, that the sintering of glass powder compacts can be variably anisotropic, i.e. the degree of anisotropy varies as sintering proceeds [8, 9]. The purpose of this work was to study the creep–densification behaviour of this class of glass powders. Experimental results on the variable anisotropic shrinkage of a barium magnesium aluminosilicate (BMAS) glass powder are evaluated in terms of creep and densification rates. Heating microscopy has been used to obtain densification data without the application of external loads under isothermal conditions. This technique has proved to be very useful for studying the sintering kinetics of both monolithic and composite powder compacts in the past [6, 7, 10–12].

2. Experimental procedure

A commercial BMAS glass powder (supplied by AEA Technology, Harwell, UK) was used in this work. The composition of this glass makes it appropriate for the production of glass-ceramics containing barium osumalite, cordierite and celsian as major crystalline phases after a suitable heat treatment [13, 14]. The theoretical density of the glass used is 2.74 $g\,cm^{-3}$; its transformation temperature, T_g, is 850 °C; the onset of crystallisation, T_n, occurs at 1150 °C, while the melting temperature $T_s \sim 1400$ °C [14]. The surface energy and the viscosity of the glass at the working temperature were determined in a previous study and found to be $\gamma \sim 0.440\ N\,m^{-1}$ and $\eta \sim 8.7 \times 10^7$ Pa s, respectively [14]. The as-received glass cullet was classified to obtain a narrow particle-size distribution, with an average particle size, r_0, of ≈ 10 μm. Scanning

‡ Also affiliated with Department of Environmental Sciences, University of Plymouth, Plymouth PL4 8AA, UK.

0022–2461

electron microscopy (SEM) was used to investigate the morphology of the glass powder. Cylindrical compacts (5 mm diameter by 5 mm) were obtained by uniaxial compression of the powder in a die without using any binder. Green densities of 51% ± 2% theoretical density were achieved using pressures of 250 MPa.

The sintering was performed in a heating microscope (Leitz Wetzlar GmbH, Wetzlar, Germany), which enabled monitoring of the axial and radial shrinkage without the application of any external load. Sintering to full density was performed in the heating microscope for 2 h at 930 °C in air. After heating the furnace to the sintering temperature the compacts were immediately placed within it in order to provide isothermal conditions over the whole sintering process. The axis of the cylindrical samples coincided with the vertical direction. At predetermined intervals during the sintering process, photographs of the samples were taken to record the samples lengths and diameters, and hence, calculate the axial and radial shrinkages.

The mass and dimensions of the pressed green and sintered compacts were measured and the geometrical densities determined. The final density of the sintered pellets was measured using Archimedes' principle, while the density as a function of time during sintering was determined from the green density and the measured shrinkage. Polished sections of a selection of the sintered cylinders were prepared parallel and normal to the axial direction. The as-polished microstructures were observed by SEM.

The instantaneous density, ρ, the longitudinal shrinkage rate, $\dot{\varepsilon}_z$, the radial shrinkage rate, $\dot{\varepsilon}_r$, the creep rate, $\dot{\varepsilon}_c$, and the densification rate, $\dot{\varepsilon}_\rho$, were calculated using the relationships given below.

From the experimental data for the axial and radial shrinkages during sintering, the density at any time can be determined by

$$\rho = \frac{\rho_0}{(1 - \Delta R/R_0)^2(1 - \Delta L/L_0)} \quad (1)$$

where $\Delta R = R_0 - R$, $\Delta L = L_0 - L$ and ρ_0 represents the green density. R_0 and L_0 are the initial radius and length, respectively, while R and L are the instantaneous radius and length, respectively, of the sample.

The data for the axial and radial shrinkages also permit the calculation of the respective shrinkage rates, $\dot{\varepsilon}_z$ and $\dot{\varepsilon}_r$, via the equations [3, 4]

$$\dot{\varepsilon}_z = \frac{d[\ln(L/L_0)]}{dt} \quad (2)$$

$$\dot{\varepsilon}_r = \frac{d[\ln(R/R_0)]}{dt} \quad (3)$$

The creep rate, $\dot{\varepsilon}_c$, and the densification rate, $\dot{\varepsilon}_\rho$, may be evaluated according to the relations [15]

$$\dot{\varepsilon}_c = 2/3(\dot{\varepsilon}_z - \dot{\varepsilon}_r) \quad (4)$$

$$\dot{\varepsilon}_\rho = \dot{\rho}/\rho = -(\dot{\varepsilon}_z + 2\dot{\varepsilon}_r) \quad (5)$$

where $\dot{\rho}$ is the derivative of the relative density with respect to the sintering time.

3. Results and discussion

Fig. 1 shows a scanning electron micrograph of the BMAS glass powder used. The particles are non-spherical with a narrow particle-size distribution. Fig. 2 shows the density as a function of the sintering time, calculated using Equation 1 with the data for the radial and axial shrinkage, and the green density. The data shown are an average of two runs under the same conditions and have a maximum relative error of 4%. The final density calculated from Equation 1 was in good agreement with the values determined using Archimedes' principle. Fig. 3 shows the results for the axial, ε_z, and radial, ε_r, shrinkage versus sintering time. The anisotropic character of the densification can be seen more clearly in Fig. 4 where the axial shrinkage has been plotted against the radial shrinkage. During sintering the samples shrank more in the radial than in the axial direction, with the ratio of axial to radial shrinkage being variable as sintering proceeds. This is in contrast to previous observations of the anisotropic shrinkage behaviour of borosilicate and aluminosilicate glass powder compacts, where the ratio of axial to

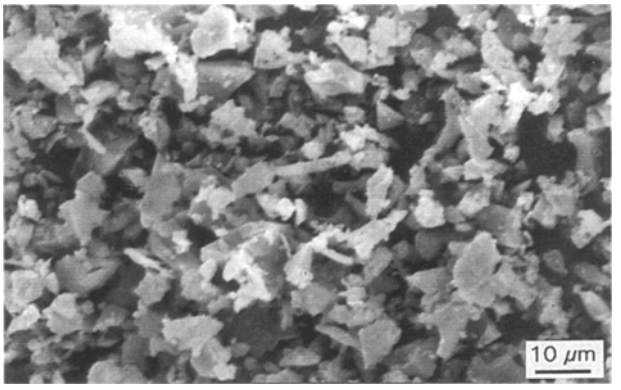

Figure 1 Scanning electron micrograph of the barium magnesium aluminosilicate glass powder investigated showing the non-spherical morphology of the particles.

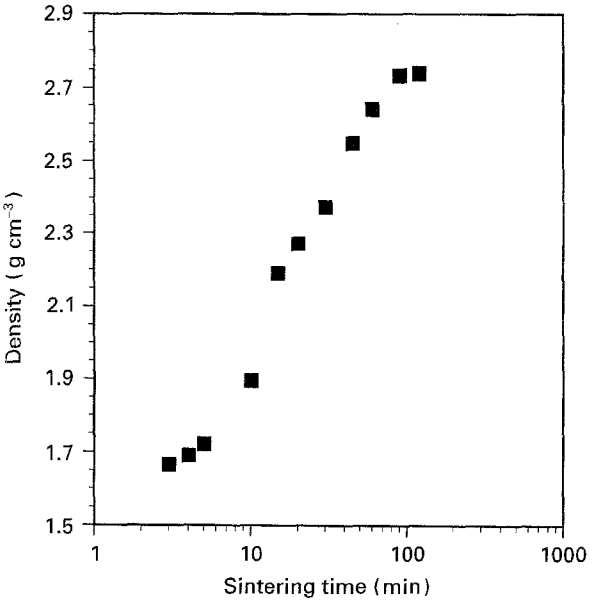

Figure 2 Density versus sintering time for BMAS glass powder compacts sintered at 930 °C, indicating that maximum density is reached after ~100 min.

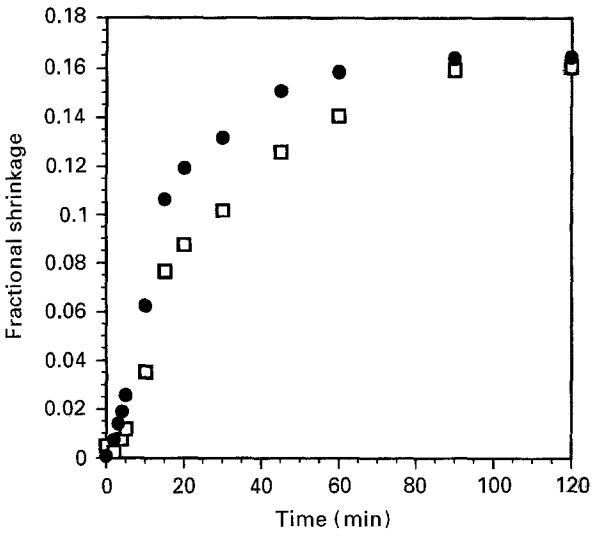

Figure 3 (□) Axial and (●) radial shrinkage of BMAS glass powder cylindrical compacts as a function of sintering time for isothermal sintering at 930 °C.

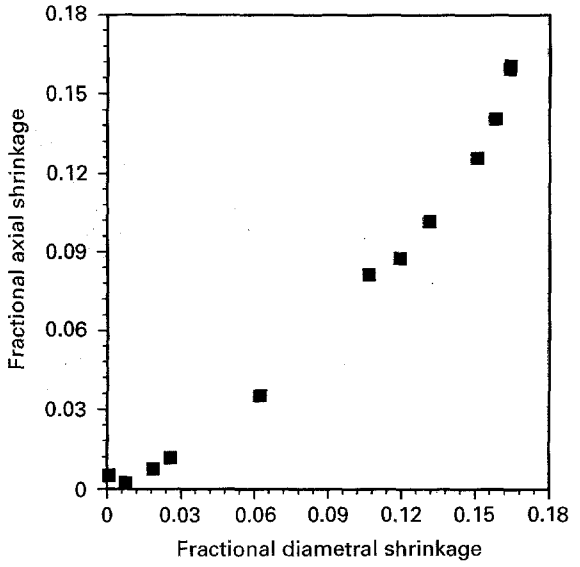

Figure 4 Relation between axial and radial shrinkage for BMAS glass powder cylindrical compacts during sintering for isothermal sintering at 930 °C indicating the anisotropic character of the shrinkage behaviour.

radial shrinkage was constant during the densification process [4, 6, 7, 12]. With the BMAS glass powder investigated here, however, this ratio varies with the degree of densification during sintering. Similar observations of varying anisotropic behaviour during sintering have been made for cordierite-type glass powders [8, 9].

A shrinkage anisotropy ratio can be defined as [16]

$$k = \frac{\varepsilon_z}{\varepsilon_r} \quad (6)$$

Fig. 5 shows the variation of the shrinkage anisotropy ratio, k, with the sintering time. Interestingly, this variation is represented by a straight line on a semi-log plot giving the following relationship between k and sintering time, t

$$k = 0.172 \ln(t) + 0.186 \quad (7)$$

with t in minutes.

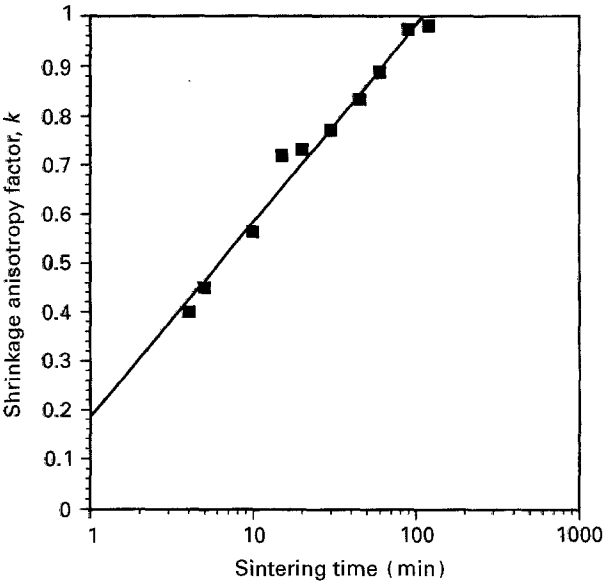

Figure 5 Shrinkage anisotropy factor, k, versus sintering time for the BMAS glass powder compacts sintered at 930 °C.

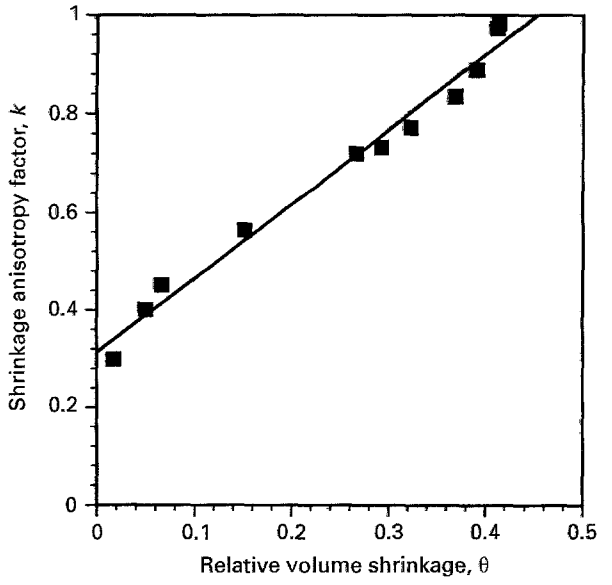

Figure 6 Shrinkage anisotropy factor, k, as a function of the relative volume shrinkage, θ, for BMAS glass powder compacts during sintering at 930 °C, showing the linear relationship between k and θ.

The progress of sintering can be followed by determining the total relative volume shrinkage, θ, which is given by

$$\theta = 1 - [(1 - \Delta L/L_0)(1 - \Delta R/R_0)^2] \quad (8)$$

By plotting the shrinkage anisotropy ratio, k, as a function of θ, the change in the shrinkage anisotropy as sintering proceeds can be assessed, as shown in Fig. 6. Shrinkage is highly anisotropic in the early stages of sintering with the relative diametral shrinkage being up to three times that of the axial shrinkage ($k \sim 0.3$). The shrinkage anisotropy factor increases continuously during sintering and reaches a value very close to 1 ($k \sim 0.98$) at full density. The variation of k with the relative volume shrinkage follows a linear relationship given by the following data-fitted equation.

$$k = 1.516\theta + 0.313 \quad (9)$$

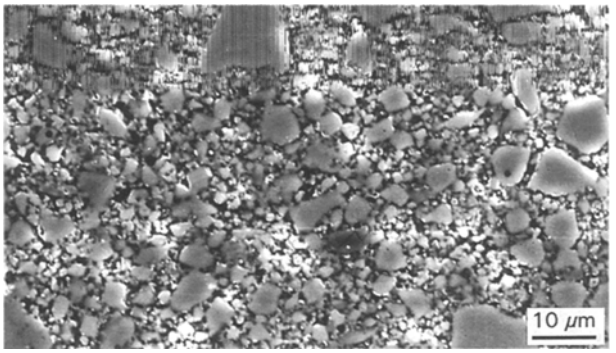

Figure 7 Scanning electron micrograph of a polished section of a compact sintered at 930 °C for 45 min (relative density $\rho_r \sim 0.72$). The sample axis corresponding to the pressing direction during powder compaction is in the vertical direction of the micrograph.

Anisotropic shrinkage behaviour is related to a number of parameters including powder particle shape, particle-size distribution, particle alignment and processing conditions (forming pressure, temperature, binder burnout, direction of gravity during sintering, etc.). An interesting stereological approach relating the anisotropic densification behaviour of glass powder compacts to the orientation of pore/solid interface has been proposed [16]. In a separate study, this approach has been applied to the BMAS glass and sintering conditions used in this work [14]. The anisotropy of the pore/solid interface during sintering can be assessed qualitatively by simple microstructural observations of the sample during sintering. Fig. 7 is a scanning electron micrograph of a polished section of a compact after 45 min sintering time having a relative density $\rho_r \sim 0.72$. While the pores show a strong scatter in shape and size, there is no visual evidence of a preferred elongation of the pores in the direction perpendicular to the cold pressing direction during the forming of the green compacts. Therefore, the anisotropy of the pore/solid interface cannot be solely responsible for the anisotropic densification behaviour of the samples investigated here. A further consideration of microstructural dependence of the shrinkage anisotropy is beyond the scope of this study. Further experimental work is being undertaken currently to elucidate the quantitative relationship between the shrinkage anisotropy factor, k, and the orientation of the pore/solid interface (which can be quantified by stereological equations [16]) in glass compacts made using high forming uniaxial pressures.

The densification rate, $\dot{\varepsilon}_\rho$, was obtained by fitting smooth curves to the data of sintered density versus sintering time plots (see Fig. 2), followed by differentiating to determine $\dot{\rho}$ and applying the following equation

$$\dot{\varepsilon}_\rho = \dot{\rho}/\rho \qquad (10)$$

The $\dot{\varepsilon}_\rho$ results derived from Fig. 2 as described previously are shown in Fig. 8 together with the results for the creep rate, $\dot{\varepsilon}_c$, which were obtained by fitting a smooth curve to the data of Figs 3 and 5, substituting Equations 6 and 9 into Equation 4 and differentiating. Likewise, the calculation of the densification rate, $\dot{\varepsilon}_\rho$, following this procedure for Equation 5 gives results that are in good agreement with the corresponding values calculated using the density data and Equation 10. The results in Fig. 8 confirm the existence of creep deformation during sintering, which, in the absence of external stresses, is due only to a shrinkage anisotropy effect as found earlier [3, 4, 6, 7]. As stated previously, the aim of this work was to show how variable shrinkage anisotropy behaviour affects the relationship between the densification and creep rates. This ratio can be written according to Equations 4–6 as

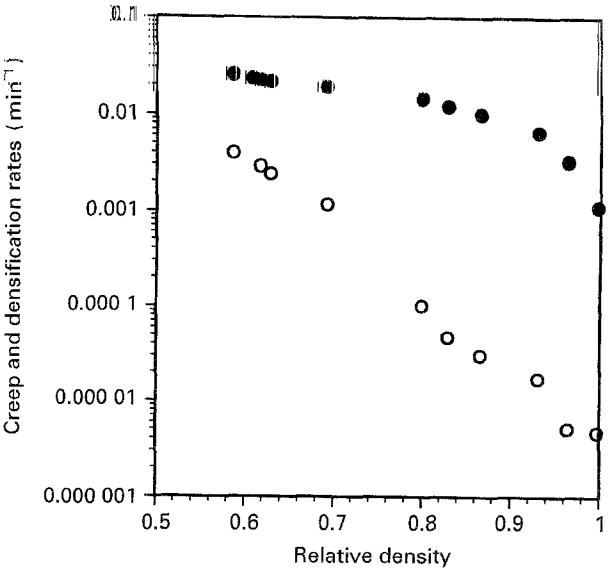

Figure 8 (●) Densification rate, $\dot{\varepsilon}_\rho$, and (○) creep rate, $\dot{\varepsilon}_c$, as a function of relative density of BMAS glass powder compacts during sintering at 930 °C.

$$\frac{\dot{\varepsilon}_c}{\dot{\varepsilon}_\rho} = \frac{2/3[\dot{k}\varepsilon_r + (k-1)\dot{\varepsilon}_r]}{[-\dot{k}\varepsilon_r - (k+2)\dot{\varepsilon}_r]} \qquad (11)$$

By means of Equations 8 and 9 and knowing that $\varepsilon_z \sim \Delta L/L_0$ and $\varepsilon_r \sim \Delta R/R_0$ [15], the relationship between ε_r and k can be found and substituted in Equation 11 to obtain the ratio of creep rate to densification rate, $\dot{\varepsilon}_c/\dot{\varepsilon}_\rho$ as a function of k and $\dot{k}$.

Equation 11 indicates a more complicated dependence of the creep rate due to anisotropic densification on the densification rate than the simple linear dependence found in the previous studies for constant shrinkage anisotropy [3, 6, 7]. Indeed, the experimental results reveal an exponential relationship between creep and densification rates during pressureless isothermal sintering as shown in Fig. 9. Furthermore, the ratio of the creep rate to the densification rate, $\dot{\varepsilon}_c/\dot{\varepsilon}_\rho$, shows a decreasing dependence with increasing densification as shown in Fig. 10. This dependence of $\dot{\varepsilon}_c/\dot{\varepsilon}_\rho$ on the density does not agree with the results of most of the previous investigations on the sintering of glass and ceramic powders for which the ratio of creep to densification rate was constant during densification [3, 4, 6, 7, 17]. An example of those results for a borosilicate glass powder sintered at 620 °C for 120 min without the exertion of external loads [6] is included in Fig. 10. Clearly the variation in the shrinkage anisotropy during the sintering of the BMAS glass compacts is the reason for this behaviour. The effects of variable shrinkage anisotropy as found in this study must, therefore, be taken into account

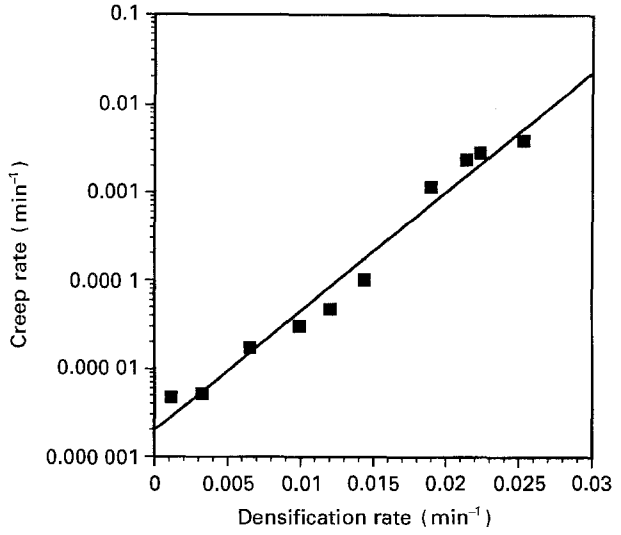

Figure 9 Relationship between the densification and the creep rates during sintering at 930 °C of the BMAS glass powder compacts.

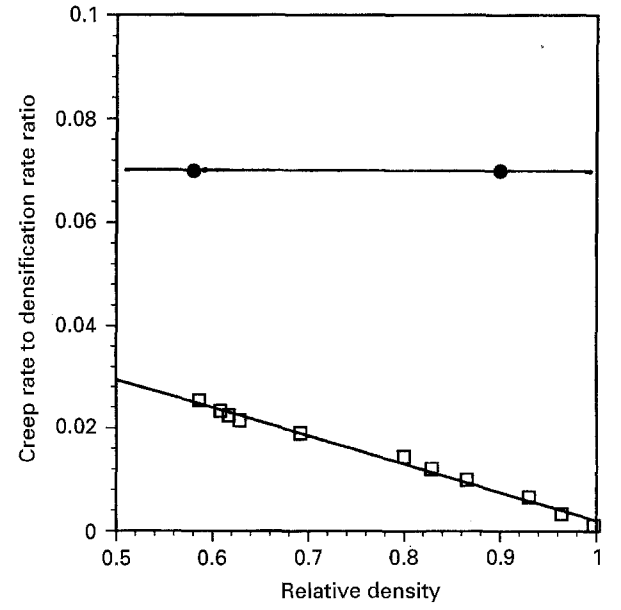

Figure 10 Ratio of creep rate to densification rate, $\dot{\varepsilon}_c/\dot{\varepsilon}_\rho$, as a function of relative density: (□) this study, (●) borosilicate glass powder sintered for 2 h at 630 °C [6].

when producing particulate-reinforced BMAS glass matrix composites by pressureless sintering. Inclusions may also have an effect on the densification and creep rates as shown for polycrystalline matrices [17]. They may introduce a new source of shrinkage anisotropy in the sintering compact, affecting, therefore, the densification behaviour of the composite due to the shrinkage anisotropy varying in a complex manner during sintering.

4. Conclusion

Heating microscopy provides an appropriate experimental method for studying the sintering kinetics of powder compacts; data for axial and radial shrinkages are obtained easily without the application of external loads, in contrast to dilatometric measurements. Thus, the sintering behaviour of samples showing shrinkage anisotropy can be studied accurately. Barium magnesium aluminosilicate glass powder compacts sintered isothermally to full density at 930 °C for 2 h showed a variable shrinkage anisotropy as sintering proceeded. According to microstructural observations the shrinkage anisotropy cannot be attributed directly to preferred microstructural orientation of the uniaxially pressed green compacts, and it varied linearly with the relative volume shrinkage. The experimental results revealed an exponential relationship between the creep and densification rates, in contrast to the linear relationship found earlier for glass compacts exhibiting constant shrinkage anisotropy. Moreover, the ratio of the creep rate to the densification rate, $\dot{\varepsilon}_c/\dot{\varepsilon}_\rho$, decreased linearly with increasing sintered density. This is also in disagreement with most previous results on glass compacts exhibiting isotropic and constant anisotropic shrinkage behaviour. Thus, variable shrinkage anisotropy during sintering is an important factor affecting the densification kinetics of glass powders. The effects of shrinkage anisotropy on the sintering behaviour of glass matrix composites with dispersion reinforcements is a subject of on-going investigations.

Acknowledgements

Dr J. Churchman-Davies, AEA Technologies, Harwell, provided the glass powders for this investigation; the heating microscopy work was carried out by Mrs W. Stumpfe at the Institut für Gesteinshüttenkunde, RWTH Aachen, Germany. The authors greatly appreciate their support. A. R. B. acknowledges the financial support of the European Commission (DGXII) with the provision of Brite-Euram contract BRE2 CT94 3064.

References

1. D. Y. JENG and M. N. RAHAMAN, *J. Mater. Sci.* **28** (1993) 4421.
2. R. K. BORDIA and R. RAJ, *J. Am. Ceram. Soc.* **69**(3) (1986) C-55.
3. M. N. RAHAMAN, L. C. DE JONGUE, G. W. SCHERER and R. J. BROOK, *ibid.* **70** (1987) 766.
4. M. N. RAHAMAN and L. C. DE JONGUE, *ibid.* **70** (1990) 707.
5. V. C. DUCAMP and R. RAJ, *ibid.* **72** (1989) 798.
6. A. R. BOCCACCINI and G. ONDRACEK, *Glastech. Ber.* **65** (1992) 73.
7. A. R. BOCCACCINI, *Bol. Soc. Esp. Ceram. Vidr.* **32** (1993) 27.
8. E. A. GIESS, J. P. FLETCHER and L. W. HERRON, *J. Am. Ceram. Soc.* **67** (1984) 549.
9. E. A. GIESS, C. F. GUERCI, G. F. WALKER *et al.*, *ibid.* **68** (1985) C-328.
10. A. R. BOCCACCINI, *Sci. Sint.* **23** (1991) 151.
11. *Idem, J. Mater. Sci.* **29** (1994) 4273.
12. *Idem, J. Mater. Sci. Lett.* **12** (1993) 943.
13. G. WEST, A. R. BOCCACCINI and D. M. R. TAPLIN, *Mattwiss. U. Werkstofftech.* **26** (1995) 368.
14. A. R. BOCCACCINI, P. A. TRUSTY and D. M. R. TAPLIN, *J. Mater. Sci. Lett.* **24** (1995) 199.
15. R. RAJ, *J. Am. Ceram. Soc.* **65** (1982) C-46.
16. H. E. EXNER and E. A. GIESS, *J. Mater. Res.* **3** (1988) 122.
17. R. E. DUTTON and M. N. RAHAMAN, *J. Mater. Sci.* **29** (1994) 1455.

Received 4 November 1994
and accepted 15 March 1995